



The Role of Submarine Groundwater Discharge to the Input of Macronutrients Within a Macrotidal Subpolar Estuary

Josianne Haag¹ · Henrietta Dulai² · William Burt^{1,3,4}

Received: 6 January 2023 / Revised: 24 May 2023 / Accepted: 18 June 2023
© The Author(s) 2023

Abstract

The major sources of macronutrients (nitrate, ammonium, phosphate, and silicic acid) in Jakolof Bay, Alaska are submarine groundwater discharge (SGD), rivers, and offshore water. We estimated SGD using natural geochemical tracers (radon and radium), a salt mass balance, and a two-component salinity mixing equation based on the change in groundwater salinity on falling lower low tide. Previous studies have hypothesized that the major macronutrient input into Jakolof Bay is offshore water. This study challenges that assumption by determining the relative contribution of macronutrients from SGD relative to offshore water and rivers. Here, SGD is tidally driven and, as the Northern Gulf of Alaska experiences some of the largest tidal ranges in the world, the SGD fluxes from this region are high relative to the global average regardless of local sediment type. The fluxes ranged from 596 ± 85 cm day⁻¹ at low tide to 97 ± 83 cm day⁻¹ at high tide and are predominantly composed of recirculated seawater (89%) rather than freshwater (11%). The major macronutrients in seawater had different input mechanisms into the semi-enclosed bay. SGD and offshore waters contend as the primary sources of nitrate, which is shown to be the limiting nutrient in this coastal area, while SGD dominates the input of silicic acid. Conversely, the aquifer is found to be a sink for phosphate, indicating that the nutrient is primarily sourced from offshore water.

Keywords Submarine groundwater discharge · Radium isotopes · Radon isotopes · Nutrients · Sub-polar

Introduction

Submarine groundwater discharge (SGD) is a dominant pathway for land-derived materials entering the ocean. Globally, SGD (fresh and saline) is three to four times greater than river discharge (Kwon et al. 2014) and transports more

nutrients to coastal ecosystems than rivers in many local studies, like the South Sea of Korea (Kim et al. 2003), the Mediterranean (Rodellas et al. 2015), and the nearshore waters off South Carolina (Crotwell and Moore 2003; Krest et al. 2000), Brazil (Niencheski et al. 2007), the Philippines (Taniguchi et al. 2008), China (Zhang et al. 2020), and Hawaii (Dulai et al. 2016). The fresh fraction of SGD (fresh SGD) is meteoric water originating as recharge from precipitation and is driven to the ocean by a hydraulic gradient in the aquifer, accounting for ~1% of the planet's freshwater flux to the ocean (Kwon et al. 2014). Globally, over 99% of total SGD is recirculated seawater (saline SGD) driven by oceanic processes such as wave pumping, wave set-up or set-down, and tidal pumping wherein seawater intruded into permeable sediments mixes with sediment pore water enriched in dissolved solutes before being drawn back into the ocean (Kwon et al. 2014).

Natural geochemical tracers are an effective method to estimate SGD-derived nutrient fluxes (Taniguchi et al. 2019). The various SGD tracers are sensitive to different processes and timescales, and the quantification of SGD through multiple independent measurements can validate the robustness

Communicated by Marco Bartoli

✉ Josianne Haag
jhaag6@alaska.edu
Henrietta Dulai
hdulaiov@hawaii.edu
William Burt
will@planetarytech.com

¹ College of Fisheries and Ocean Sciences, University of Alaska Fairbanks, Fairbanks, AK 99775, USA

² Department of Earth Sciences, University of Hawaii, Honolulu, HI 96822, USA

³ Planetary Technologies, Dartmouth, NS B2Y 4W6, Canada

⁴ Department of Oceanography, Dalhousie University, Halifax, NS B3H 3Z1, Canada

of results. Radium (Ra) is a chemical proxy for SGD as it is continuously produced by the decay of parental isotopes that are found primarily in soils, sediments, and rock. The four naturally occurring Ra isotopes (^{224}Ra , ^{223}Ra , ^{228}Ra , and ^{226}Ra) range widely in half-lives (3.6 days, 11.4 days, 5.8 years, and 1600 years, respectively) and can be used at a variety of oceanographic process timescales (Moore 2003). Ra is a particle-reactive alkaline earth metal that adsorbs to iron and manganese-oxides formed in oxidizing environments such as sediment modified by redox reactions (Eröss et al. 2012; Lecher et al. 2016b) but desorbs from sediments through cation exchange with dissolved ions in seawater that percolates into the aquifer through seawater intrusion (Garcia-Orellana et al. 2021). The noble gas radon (Rn) is another useful tracer of SGD because it is highly concentrated in coastal aquifers (due to continual decay of its parent Ra isotope) relative to seawater (due to losses from decay and atmospheric evasion). This rapid Rn loss also means that measured seawater Rn inventories represent recent inputs, allowing for the determination of relatively instantaneous groundwater fluxes (Burnett and Dulaiova 2003).

The Northern Gulf of Alaska (NGA) contains one of the largest tidal ranges in the world which drives large saline SGD fluxes (Archer 2013; Lecher et al. 2016a; Dimova et al. 2015). However, the Alaskan coastline is highly diverse, ranging from rocky to sandy beaches and mudflats, and to varying degrees of exposure to wave action depending on open coastline versus semi-enclosed bays (Field and Walker 2003), and SGD can vary greatly between these locations due to differences in sediment permeability, strength of wave/tidal pumping, and slope of the water table (Virtasalo et al. 2019; Santos et al. 2021). To date, prior SGD work in the NGA is limited to a partially exposed rocky beach, where SGD was found to be a source of nitrate, silicic acid, iron, and nickel (Lecher et al. 2016a, b, 2017; Dimova et al. 2015). Lecher et al. (2016b) concluded that Alaskan SGD nutrient fluxes can rival those of rivers across the entire NGA. However, neither rivers nor SGD are considered the main sources of nutrients to the NGA, instead macronutrients are primarily sourced from offshore topographic steering, eddies, and upwelling (Childers et al. 2005). In semi-enclosed bays, where the degree of advection from offshore water may be limited, SGD is likely to play an enhanced role in supplying macronutrients to the nearshore water. Comparison of the relative contributions of offshore water to SGD and river input is needed to fully understand the nutrient dynamics in semi-enclosed bays along this coastline, as it can influence the base of marine food webs (Lecher et al. 2017).

This study tested the hypothesis that tidally driven SGD is a dominant source of macronutrients in a semi-enclosed bay with extensive mudflats (Jakolof Bay). Due to the complexity of the nearshore system with expected variety of SGD pathways, multiple independent approaches

were employed: the total SGD was estimated from a ^{222}Rn mass balance model and a ^{224}Ra mass balance model. Fresh SGD was estimated from a salt mass balance model and a two-component mixing equation based on the decrease in groundwater salinity on a falling lower low tide. As a critical component of the Ra mass balance, water residence time was estimated using a tidal prism model. SGD estimates were compared to a neighboring embayment with a rocky beach (Kasitsna Bay), which to the best of our knowledge, represents the only other tracer-based groundwater study conducted in the NGA. Finally, we evaluated the relative importance of groundwater and offshore water as sources of essential macronutrients to Jakolof Bay.

Methods and Materials

Study Area

Jakolof Bay (59.4469, -151.5103), a semi-enclosed estuary dominated by extensive mudflats (Fig. 1), is adjacent to Kasitsna Bay (see Fig. 1), the site of the only tracer-based submarine groundwater discharge (SGD) estimates in the region (Lecher et al. 2016a; Dimova et al. 2015). Both bays possess features that may be conducive to high SGD. Saline SGD is driven by some of the greatest tidal ranges in the world (up to 8 m; Archer 2013). Meanwhile, the fresh fraction is driven by a steep hydraulic gradient created by precipitation and high topographical relief (max elevation = 1140 m, mean elevation = 502 m). The annual precipitation during our study was 601 mm in 2020 and 569 mm in 2021 (NOAA National Weather Service 2023). However, within Jakolof Bay, highly impermeable mudflats, which are composed of roughly 60% fine grained clay and silt (Hartwell et al. 2016), may limit the recirculation of seawater through the sediment and constrict SGD flow to areas of coarser sand. According to Miller and Kelley (2021a), the topography in this bay suggests minimal fresh SGD, and that porewater intrusion is likely dominated by seawater during flood tide.

Unlike most watersheds in Alaska, the heavily forested (64%) watershed feeding into Jakolof River is small (19 km²) and disconnected from the Harding Ice Field; therefore, the river can dry out by late July after heavy rainfall has stopped and the annual snowpack has melted. The river discharge in this bay is low, and ranged between a spring maximum of 2.49 m³ s⁻¹ in late May 2021 to zero in August 2021 (annual average in 2021 was 0.72 m³ s⁻¹; Jenckes et al. 2023). The source of nutrients in Jakolof Bay presumably varies seasonally, with tidal mixing of advected, seasonally nutrient-rich Alaska Coastal Current (ACC) being the primary origin of macronutrients in spring and autumn (Childers et al. 2005). In the late summer, with little-to-no riverine input, terrestrial nutrients are likely to be introduced

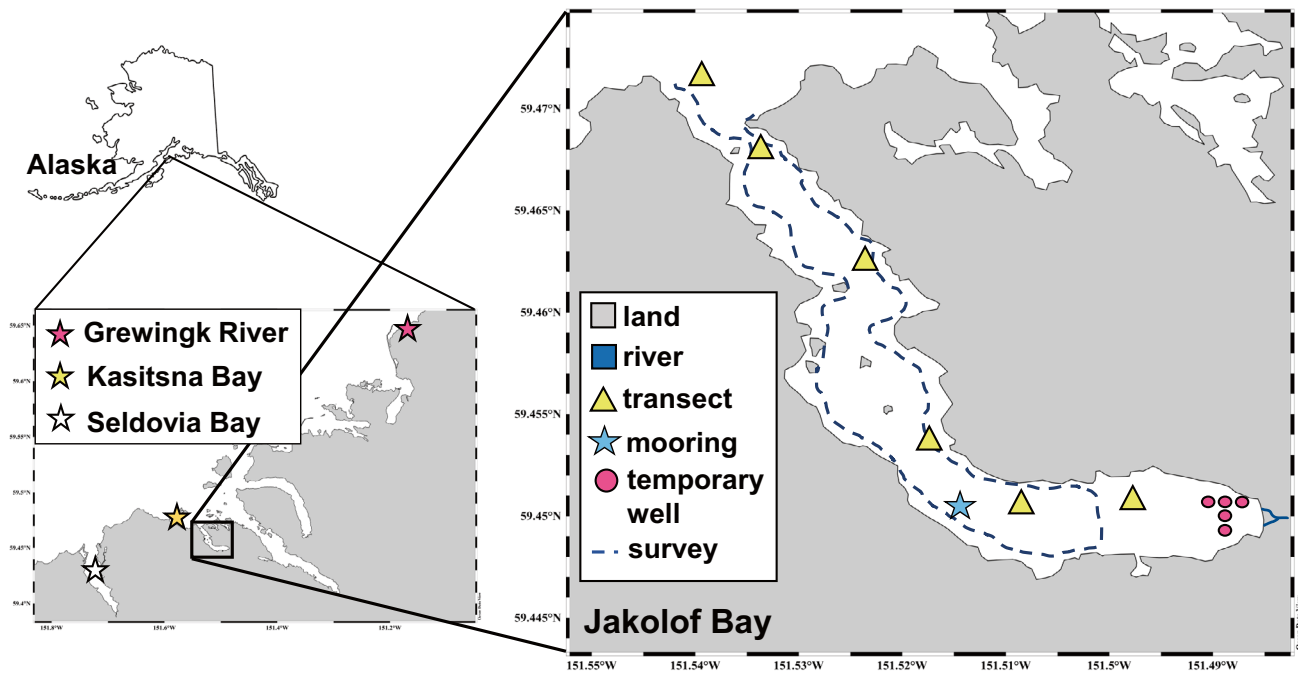


Fig. 1 Map of the study area sampled during three seasons at neap tide: September 2020, May 2021, and July 2021. The location of the Ra transects repeated every season is marked by triangles, the 12-h ^{222}Rn mooring in summer with hourly CTD casts for the water column salinity is marked by a star, the temporary wells for measuring ^{222}Rn and

^{224}Ra variability in groundwater in spring is marked by circles, and the ^{222}Rn survey of the perimeter of the bay at low tide and high tide in spring is marked by a dashed line. The river station in spring was (59.4502, -151.4867) and in summer was (59.4494, -151.4876)

predominantly through SGD. Physical mixing of the water column in Jakolof Bay is due to the local wind field controlled by (1) seasonal storm activity in the NGA, (2) daily pressure differentials between the land and ocean, and (3) the flow of cold air from the Harding Ice Field (Field and Walker 2003). At times, the long, narrow bay acts as a wind tunnel that allows for strong overturning of the water column that can distribute nutrients throughout the bay.

Sample Strategy

Our field campaign was conducted at neap tide during three seasons: autumn (21 to 25 September 2020), spring (12 to 22 May 2021), and summer (10 to 18 July 2021). While most sampling focused on Jakolof Bay for logistical reasons we also extended sampling into the neighboring Kasitsna Bay where a permanent dock facilitated longer monitoring of tidal dynamics of SGD.

Radon and Radium Measurements in Seawater

Two types of ^{222}Rn measurements were performed: a spatial survey, to find SGD variability along the shoreline, and continuous tidal monitoring to assess SGD variability with changing tides. To determine the spatial distribution of SGD, we conducted two ^{222}Rn surveys around Jakolof

Bay using a Rn-in-air monitor (Durrige Co., Inc. RAD-7) with the RAD-Aqua attachment deployed on a boat moving at $< 5 \text{ km h}^{-1}$ in spring 2021, once at low tide and once at high tide (Fig. 1). We measured ^{222}Rn continuously in 5-min intervals and tracked the survey path using a Garmin inReach GPS unit (Datum WGS84).

Tidal dynamics of SGD were derived from a continuous ^{222}Rn measurement, where a RAD-Aqua received a continuous flow of water from a submersible pump fixed at 0.5 m depth from an anchored zodiac for 12 h in Jakolof Bay (6:45 to 18:45 on July 17, 2021) (Fig. 1). The ^{222}Rn data was integrated over 1-h intervals to reduce uncertainty to $< 10\%$. Every hour during this deployment, a CTD was lowered to obtain temperature, salinity, and oxygen data. A second RAD-7 ran concurrently to measure atmospheric ^{222}Rn activities and, coupled with wind speed gathered from Willy Weather (<https://wind.willyweather.com/ak/kenai-peninsula-borough/jakolof-bay-airport.html>), provided the ^{222}Rn loss through gas evasion. The Jakolof Bay mooring could only extend for 12 h, and we included a longer time-series of ^{222}Rn measurements at the Kasitsna Bay dock during September 24 and 25, 2020, to demonstrate the variation in ^{222}Rn activity over multiple tidal cycles.

To obtain another independent estimate of total SGD in Jakolof Bay, we measured Ra isotopes along a 6-station transect during each season, collecting surface Ra, nutrients,

temperature, and salinity (Fig. 1). All six surface Ra samples were analyzed for ^{224}Ra , but only three were selected for the longer-lived ^{226}Ra analysis, due to isotope counting constraints. In spring, we conducted the transect twice: once at low tide and once at high tide. To obtain reliable estimates of Ra, large-volume samples (> 100 L) were taken from 0.5 m depth below water surface.

River Water, Groundwater, and Offshore Observations

One must consider all possible inputs of ^{222}Rn and Ra tracers into the bay. These include diffusion from sediments, in situ production of radon from its parent, and input by rivers and from offshore. ^{222}Rn in river and offshore waters were measured using the RAD-Aqua deployed for at least 30 min, and river discharge was measured by collaborators (Jenckes et al. 2023). Radon produced from its Ra parent was derived from the measured ^{226}Ra activities.

To estimate the diffusive flux of ^{222}Rn and ^{224}Ra from the sediment, wet sediment was collected from the Jakolof Bay mudflat. For the ^{222}Rn experiment, 80 g of wet sediment sample was sealed with ~230 mL of deionized water for 20 days for ^{222}Rn and ^{226}Ra to reach radioactive decay equilibrium before analysis on a RAD-H₂O (Corbett et al. 1997; Dabrowski et al. 2020). For the ^{224}Ra experiment, we filled a 1 L graduated cylinder with sediment to > 20 cm depth. After 8 days, the overlying seawater was processed, and we estimated the flux of ^{224}Ra from the seafloor (F_{sed}) to be equal to:

$$F_{sed} \left(\frac{\text{Bq}/\text{m}^3}{\text{m}^2 \text{ day}} \right) = \frac{\left[{}^{224}\text{Ra} \left(\frac{\text{Bq}}{\text{m}^3} \right) \right]}{t \text{ (day)} \times \pi r^2 \text{ (m}^2\text{)}}$$

where ^{224}Ra was the measured ^{224}Ra activity in the overlying seawater, t was the duration of the experiment, and r was the radius of the graduated cylinder. This technique may lead to greater diffusive fluxes than incubating an intact sediment core, but it also neglects the effects of resuspension and bioturbation which would increase the diffusion rate.

Groundwater endmembers were collected by first deploying five temporary wells (following methods described by Lecher et al. 2016a and Krest et al. 2000) two meters deep in the upper mudflats of Jakolof Bay in spring 2021 and one well in summer 2021. We drilled holes in the bottom foot of a PVC pipe and covered the spaces with a mesh (1 mm). The well was wide enough to fit an Onset HOB0 conductivity logger, calibrated as seen in Miller and Kelley (2021b), to track the salinity and temperature of the surface aquifer over multiple tidal cycles. ^{224}Ra and ^{222}Rn groundwater endmembers were collected from these wells using a submersible pump in spring and summer 2021.

A major Ra input along with SGD is its desorption from suspended sediments carried by rivers. To determine the relationship between adsorbed Ra and salinity in river water, we performed a river desorption experiment. On May 14, 2021, five 100 L samples of water from nearby Grewing River (59.6397, -151.1642; see Fig. 1) were taken, and NaCl was added to each sample to span the following salinities: 0, 5, 10, 15, and 20. As later shown, full desorption of Ra from the riverine suspended particles occurred at salinity 15, thus the Jakolof River spring and summer Ra samples were raised to salinity 20 to account for the fraction of the tracer desorbing from riverine suspended solids.

Endmember nutrient concentrations were taken from river water and groundwater in all three seasons (except for groundwater in autumn). Offshore nutrient concentration estimates were taken from the first station of the historic Seward Line (GAK1) during two cruises: spring 2021 (April 23), and summer 2021 (June 28) (Ana Aguilar-Islas, pers. comm.) in an effort to represent the offshore waters supplied by upwelling (Childers et al. 2005). The data did not include ammonium, so this nutrient was not included in our comparison between SGD and offshore water nor the N:P. We utilized nutrient samples taken a month prior to Jakolof Bay fieldwork to compensate for water transit times from GAK1 to our study site. The offshore nutrient data was integrated over the top 75 m of the water column. Monthly nutrient concentration from Seldovia Bay, a bay < 10 km from Jakolof Bay (Fig. 1), in 2019 was provided by the NOAA National Estuarine Research Reserve System (2021).

Analytical Methods

Radium Analysis

Ra samples were passed through a cartridge filled with 25 g of MnO₂-coated acrylic fiber at < 1 L min⁻¹. We placed two cartridges in series to determine our extraction efficiency to be 89 ± 3% ($n = 3$) and corrected the Ra data to account for the 11% loss. Short-lived ^{224}Ra was measured in the field on a Radium Delayed Coincidence Counter (RaDeCC) calibrated with a standard within 2 days of sample collection and recounted 2 months later at the University of Alaska Fairbanks (UAF) to correct for the ^{228}Th supported ^{224}Ra (Garcia-Solsona et al. 2008; Charette and Buesseler 2004). Samples of the long-lived isotope ^{226}Ra were analyzed by ashing the fibers at 800 °C for 10 h, sealing them for 21 days, and measuring them on a gamma spectrometer at the University of Hawaii at Mānoa (Charette and Buesseler 2004). The seawater ^{223}Ra activity was low, resulting in large uncertainties (> 100%), and thus is not reported.

Nutrient Analysis

The 20 mL nutrient samples were filtered through a 0.45 μm nitrocellulose membrane filter and stored frozen in acid cleaned HDPE bottles, then thawed samples were analyzed using a Seal Analytical continuous-flow QuAAtro39 Auto-Analyzer at UAF (Armstrong et al. 1967; Murphy and Riley 1962; Kerouel and Aminot 1997).

Mass Balance Calculations

Water Residence Time Estimation

To calculate water residence time, we used the tidal prism method by Wang et al. (2015) that compared the water volume in the bay at low tide versus high tide. We split Jakolof Bay into evenly spaced crosswise slices and assumed each subsection resembled a triangular prism. Using the depth data from the bay transects, we summed the subsections at high tide and low tide. The difference between these two time points was the tidal prism (P_{tide}) and the average of the two was the average total volume of Jakolof Bay (V_{bay}). Thus, the water residence time (τ) was calculated:

$$\tau \text{ (sec)} = \frac{V_{\text{bay}} \text{ (m}^3\text{)}}{Q_{\text{river}} \left(\frac{\text{m}^3}{\text{sec}}\right) + Q_{\text{mixing}} \left(\frac{\text{m}^3}{\text{sec}}\right)}$$

where Q_{river} is river discharge and Q_{mixing} is offshore mixing as calculated by:

$$Q_{\text{mixing}} \left(\frac{\text{m}^3}{\text{sec}}\right) = \frac{P_{\text{tide}} \text{ (m}^3\text{)}}{\text{time of tidal cycle (sec)}}$$

Radon-Based Total SGD Estimation

Total SGD estimates were calculated using a ^{222}Rn mass balance model (Burnett and Dulaiova 2003; Wu et al. 2013). We first converted the ^{222}Rn timeseries data (Rn_{measured}) to the normalized inventory (I_{net}):

$$I_{\text{net}} \left(\frac{\text{Bq}}{\text{m}^2}\right) = \left(Rn_{\text{measured}} \left(\frac{\text{Bq}}{\text{m}^3}\right) - Rn_{\text{supported}} \left(\frac{\text{Bq}}{\text{m}^3}\right)\right) \times d \text{ (m)}$$

$$F_{\text{net}} \left(\frac{\text{Bq}}{\text{m}^2 \text{ hr}}\right) = \frac{I_{\text{net},t2} \left(\frac{\text{Bq}}{\text{m}^2}\right) - I_{\text{net},t1} \left(\frac{\text{Bq}}{\text{m}^2}\right)}{t_2 \text{ (hr)} - t_1 \text{ (hr)}}$$

where $Rn_{\text{supported}}$ is the ingrowth from ^{226}Ra which is assumed to be in secular equilibrium with its daughter isotope, d is the water depth, and t_1 and t_2 are consecutive time-points of the timeseries. Positive F_{net} values indicate low

tide and negative F_{net} values indicate high tide. F_{net} must be corrected for other ^{222}Rn sources and sinks contributing to its inventory (F_{net}^*):

$$F_{\text{net}}^* \left(\frac{\text{Bq}}{\text{m}^2 \text{ hr}}\right) = F_{\text{net}} \left(\frac{\text{Bq}}{\text{m}^2 \text{ hr}}\right) + / - \Delta d \times Rn_{\text{off/near}} \left(\frac{\text{Bq}}{\text{m}^2 \text{ hr}}\right) + F_{\text{atm}} \left(\frac{\text{Bq}}{\text{m}^2 \text{ hr}}\right) - F_{\text{river}} \left(\frac{\text{Bq}}{\text{m}^2 \text{ hr}}\right) - F_{\text{sed}} \left(\frac{\text{Bq}}{\text{m}^2 \text{ hr}}\right) - F_{\text{mix}} \left(\frac{\text{Bq}}{\text{m}^2 \text{ hr}}\right)$$

where Δd is the unit change in water depth over the measured interval. If Δd is positive, it is multiplied by the offshore ^{222}Rn activity (Rn_{off} ; 6.6 Bq m^{-3}) but if Δd is negative, it is multiplied by the nearshore ^{222}Rn activity (Rn_{near} ; excess ^{222}Rn from that timepoint in the timeseries). The atmospheric gas evasion flux (F_{atm}) is calculated from MacIntyre et al. (1995), using a gas transfer coefficient (k) that accounts for wind speed and air temperature. In the absence of wind during the first 4 h of the moored timeseries in Jakolof Bay, atmospheric evasion did not stop entirely, therefore k was assumed to be $0.8 \pm 0.5 \text{ cm h}^{-1}$ (Happell et al. 1993).

The river flux (F_{river}) is ignored for the summer timeseries due to the circulation of the bay as the river discharge exits the bay along the northern shore. The sediment diffusion flux (F_{sed}) was calculated via lab incubation. The radioactive decay flux was not considered as the hourly fluxes were evaluated on a short timescale relative to the half-life of ^{222}Rn (3.8 days) (Burnett et al. 2008).

Then F_{net}^* was converted to SGD flux:

$$\text{SGD} \left(\frac{\text{cm}}{\text{day}}\right) = \frac{F_{\text{net}}^* \left(\frac{\text{Bq}}{\text{m}^2 \text{ hr}}\right) + F_{\text{mix}} \left(\frac{\text{Bq}}{\text{m}^2 \text{ hr}}\right)}{Rn_{\text{gw}} \left(\frac{\text{Bq}}{\text{m}^3}\right)} \times \frac{100 \text{ cm}}{\text{m}} \times \frac{24 \text{ hr}}{\text{day}}$$

where Rn_{gw} is the greatest measured ^{222}Rn activity in groundwater and F_{mix} is the ^{222}Rn loss via advective mixing with lower ^{222}Rn activity offshore water based on the maximum negative net flux (F_{net}^*) (Burnett and Dulaiova 2003), which we show later to be comparable to an F_{mix} estimated using the tidal prism-based water residence time for inner Jakolof Bay. SGD is multiplied by the seepage face of the mudflat at the head of Jakolof Bay to convert from units of cm day^{-1} to $\text{m}^3 \text{ s}^{-1}$ to compare these values to other fluxes calculated for the bay. The seepage face was estimated by tracing the area where most of the SGD flux is likely to occur, in the case of Jakolof Bay it is the Quaternary surficial deposits at the head of the bay in the intertidal zone (Schmoll et al. 1984), and using Pythagorean's theorem and the average slope of the bathymetry (50°) to calculate a final value of $707,000 \pm 180,000 \text{ m}^2$ (Aeon Russo, pers. comm.).

Radium-Based Total SGD Estimation

Total SGD estimates were calculated using a ^{224}Ra mass balance model:

$$SGD \left(\frac{m^3}{s} \right) = \frac{F_{decay} \left(\frac{Bq}{sec} \right) - F_{river} \left(\frac{Bq}{sec} \right) - F_{sed} \left(\frac{Bq}{sec} \right) + / - F_{mix} \left(\frac{Bq}{sec} \right)}{Ra_{gw} \left(\frac{Bq}{m^3} \right)} \times$$

$$F_{mix} \left(\frac{Bq}{sec} \right) = \frac{V_{bay}(m^3)}{\tau(sec)} \left(Ra_{bay} \left(\frac{Bq}{m^3} \right) - Ra_{off} \left(\frac{Bq}{m^3} \right) \right)$$

where F_{decay} is the radioactive decay flux, F_{river} is the river flux whose salinity was increased to 20 to ensure total desorption from the suspended particles (based on the river desorption experiment), F_{sed} is the sediment diffusion flux calculated by a lab experiment, F_{mix} is the mixing between the bay water and offshore water which is a positive or negative value depending on the tidal stage, and Ra_{gw} is the Ra groundwater endmember. F_{mix} is calculated by τ which is the entire bay's tidal prism-based water residence time, Ra_{bay} which is the Ra activity in the bay, and Ra_{off} which is the Ra activity in offshore waters. If Ra_{bay} was greater than Ra_{off} , offshore water served as a sink of Ra and F_{mix} was positive; however, if Ra_{bay} was greater than Ra_{off} , offshore water served as a source of Ra and F_{mix} was negative.

The ^{224}Ra groundwater endmember in spring was the average ^{224}Ra activity measured in groundwater ($n=7$) and in summer only one measurement was taken. No groundwater sample was taken in autumn; thus, we used the average ^{224}Ra activity in groundwater from spring and summer.

Fresh SGD Estimation

Fresh SGD estimates were calculated using two different methods. The first way followed a similar set of equations as the total ^{222}Rn -based SGD (Burnett and Dulaiova 2003):

$$FSGD_{net} \left(\frac{cm}{day} \right) = \frac{\bar{d} (cm)}{\tau (day)} \times \left(1 - \frac{S_2}{S_1} \right)$$

where \bar{d} is the average depth of the water column over a 1-h interval, τ is the water residence time of the inner bay as this mooring was taken near the mudflats at the head of the bay, and S_1 and S_2 is the average salinity of the water column between one timepoint and another taken an hour apart. The depth considered above, and its respective salinity, had the top meter of the water column removed in order that the freshwater input from surface sources was not considered in this mass balance. As the presence of the river discharge in the surface water depended on the tidal cycle, estimating the contribution of the exact river discharge to the upper water column every hour is difficult. The greatest negative $FSGD_{net}$ was considered as the loss of fresh water through

mixing with offshore water ($FSGD_{mix}$) and a final fresh SGD flux was calculated:

$$FSGD \left(\frac{cm}{day} \right) = FSGD_{net} \left(\frac{cm}{day} \right) + FSGD_{mix} \left(\frac{cm}{day} \right)$$

The second fresh SGD estimate was calculated using a method from Dimova et al. (2015) by analyzing the linear decrease in salinity in a well over an ebb tide:

$$FSGD \left(\frac{cm}{day} \right) = \frac{V_{well} (cm^3)}{t (day) \times \pi r_{well}^2 (cm^2)} \left(1 - \frac{S_f}{S_i} \right)$$

where V_{well} is the average volume of groundwater in the well, S_i and S_f are the initial and final salinity values of the groundwater in the well over the ebb tide, t is the time between salinity measurements, and r_{well} is the radius of the well.

Statistical Analysis

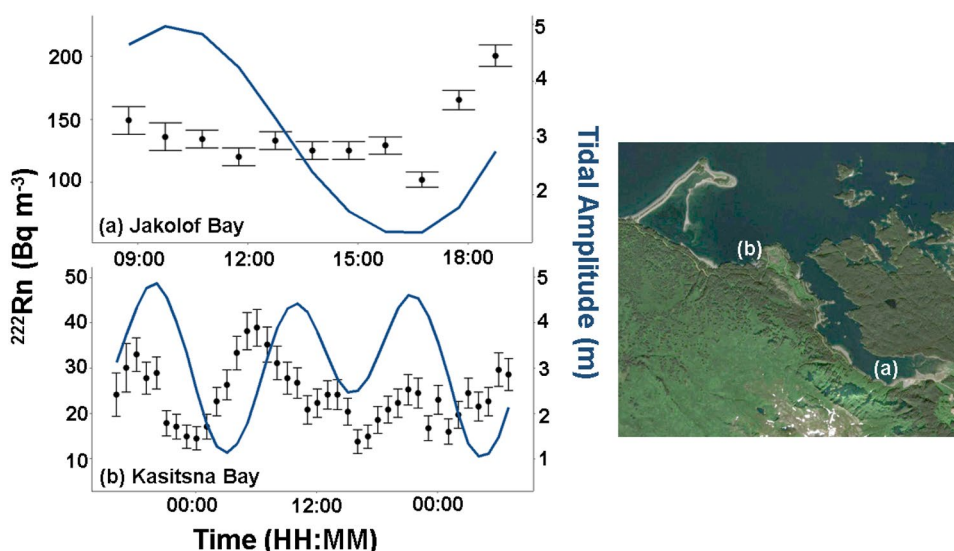
Statistical tests were performed in R (version 4.2.1) with the RStudio Workbench (R Core Team 2022). We did an autocorrelation (function `acf`) to determine the lag between ^{222}Rn in surface seawater and the tidal amplitude. Following a Shapiro Wilk's test for normality and a Bartlett test for equal variance, differences between seasonal nutrient concentrations were determined using an ANOVA ($p < 0.05$). If significance was found, this test was followed by a post-hoc Tukey–Kramer test ($p < 0.05$) to determine which seasonal nutrient concentrations were significantly different from the others. If normality was not found, a Kruskal–Wallis test was used to determine the difference in seasonal nutrient concentrations, and a Dunn Test was performed as a post-hoc test.

Results

Radon and Radium in Seawater

The moored timeseries in Jakolof Bay on July 17th, 2021, revealed variations in excess ^{222}Rn inventory in surface seawater ranging from 103 Bq m⁻³ to 201 Bq m⁻³ while the Kasitsna Bay timeseries yielded an order of magnitude lower range of excess ^{222}Rn from 13.9 Bq m⁻³ to 38.9 Bq m⁻³. The tidal height modulated the ^{222}Rn activity, with greater activities of the tracer at low tide and vice versa (Fig. 2). A cross-correlation between tidal height and ^{222}Rn activity at Kasitsna Bay yielded a lag of 3 h. A cross-correlation could not be made for the limited timeseries in Jakolof Bay as it only spanned one tidal cycle; hence, we estimated the lag at the mudflat to be 7 h assuming this was the difference between low tide and the peak of ^{222}Rn as seen with the cross-correlation in Kasitsna Bay (Fig. 2).

Fig. 2 Variation in total excess ^{222}Rn activity (Bq m^{-3}) in the ambient seawater with tidal change at **a** Jakolof Bay on July 17th, 2021, and **b** Kasitsna Bay from September 24 to 26, 2020. The ^{222}Rn activity is represented by the dots with standard error as the error bars and the tidal amplitude is represented by the line



The boat surveys revealed excess surface water ^{222}Rn activities that were considerably lower than the moored timeseries in Jakolof Bay (Fig. 3). The average measured excess ^{222}Rn during the high tide survey was $9.6 \pm 3 \text{ Bq m}^{-3}$ ($n=9$), an order of magnitude lower than during the low tide survey ($62 \pm 21 \text{ Bq m}^{-3}$; $n=7$) (Fig. 3). The error associated with each measurement in the survey was $\sim 50\%$ due to low counts measured on the RAD-7.

There was a rapid log-linear decline in ^{224}Ra activities with distance from the head of Jakolof Bay across seasons, and between low and high tide (R^2 ranged from 0.75 to 0.90; Fig. 4). The conservative nature of ^{224}Ra activity across the bay showed that the primary source of the tracer was from the head of the bay. The ^{224}Ra activities in surface seawater were lower at high tide in spring ($0.15 \pm 0.03 \text{ Bq m}^{-3}$, $n=6$), relative to autumn ($0.32 \pm 0.05 \text{ Bq m}^{-3}$, $n=6$), spring at low tide ($0.21 \pm 0.03 \text{ Bq m}^{-3}$, $n=5$), and summer ($0.28 \pm 0.04 \text{ Bq m}^{-3}$, $n=6$) (Fig. 4). The furthest station from the head of the mudflat had similar ^{224}Ra activities across

all three seasons and high and low tide ($0.13 \pm 0.02 \text{ Bq m}^{-3}$, $n=4$) so this value was used as the ^{224}Ra activity of offshore water. Seawater ^{224}Ra activity was generally lower than river water and groundwater (Fig. 5).

Radon and Radium Endmembers

River Observations

The results of the river desorption experiment from Grewingk River (Fig. 1) yielded a linear relationship between ^{224}Ra activity and salinity ($R^2=0.98$, $n=4$, p -value=0.007) until a salinity of 15, where the ^{224}Ra activity no longer increased (Fig. 6). The difference between the ^{224}Ra activity at salinity 0 and salinity 15 showed that 83% of the riverine ^{224}Ra budget was unaccounted for if only a dissolved ^{224}Ra sample was taken. The ^{224}Ra that desorbed from riverine suspended solids in higher salinity seawater must be considered to constrain the input of ^{224}Ra from rivers.

Fig. 3 The ^{222}Rn boat surveys conducted at high tide and low tide in Jakolof Bay on May 17th 2021 and May 22nd, 2021, respectively. The depth-corrected ^{222}Rn inventory was greater on average at low tide than high tide, indicating a higher SGD flux

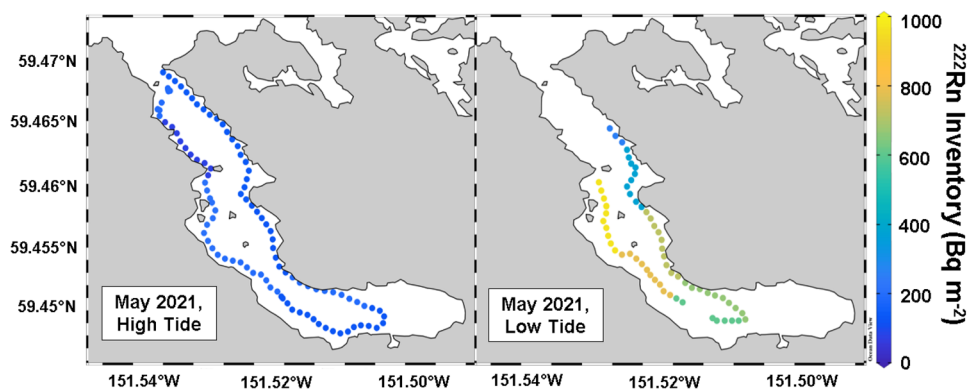
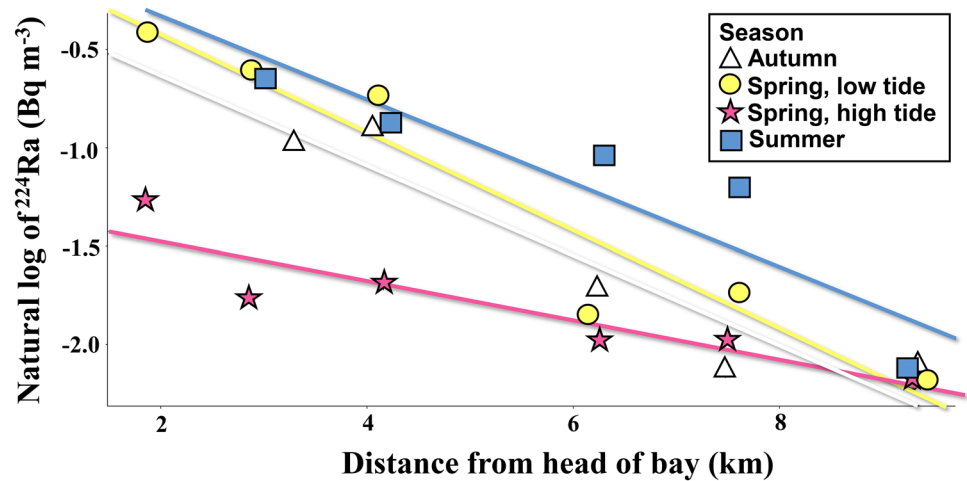


Fig. 4 The fitted linear regression of the natural log of ^{224}Ra and distance from the head of the bay has an R^2 value of 0.90 in autumn, 0.85 in spring at low tide, 0.78 in spring at high tide, and 0.75 in summer



Groundwater Observations

In spring, the groundwater ^{222}Rn activities ranged from 489 to 1680 Bq m^{-3} (average = $947 \pm 499 \text{ Bq m}^{-3}$), with no relationship to salinity ($R^2 = 0.0038$, $n = 7$, $p = 0.913$; Fig. 7). To ensure more conservative springtime SGD flux estimates, we used the highest measured ^{222}Rn activity for the spring SGD flux estimates ($1680 \pm 150 \text{ Bq m}^{-3}$). This higher value aligned well with the summertime groundwater ^{222}Rn activity measured from a single well ($1850 \pm 60 \text{ Bq m}^{-3}$) which was applied for summer total SGD estimates. In contrast to ^{222}Rn , a robust linear relationship existed in spring between groundwater ^{224}Ra activity and salinity ($R^2 = 0.86$, p -value = 0.002, $n = 7$; Fig. 7). The activity of ^{224}Ra in spring groundwater ranged from $0.6 \pm 0.01 \text{ Bq m}^{-3}$ at salinity 0.3 to $1.52 \pm 0.06 \text{ Bq m}^{-3}$ at salinity 5.2 (average = $0.61 \pm 0.12 \text{ Bq m}^{-3}$, $n = 7$) and the summer sample was taken at salinity 2.6 ($0.84 \pm 0.04 \text{ Bq m}^{-3}$).

Nutrients

The concentration of different macronutrients varied between groundwater, river water, and seawater. The average nitrate (NO_3^-) concentrations in Jakolof Bay were greatest for river water ($15.21 \pm 6.69 \mu\text{M}$), and lowest in seawater ($3.91 \pm 2.02 \mu\text{M}$), with groundwater falling in between ($6.50 \pm 2.25 \mu\text{M}$) (Fig. 8). The average ammonium (NH_4^+) concentrations in Jakolof Bay were greatest for seawater ($1.05 \pm 0.27 \mu\text{M}$), and lowest in river water ($0.33 \pm 0.17 \mu\text{M}$), with groundwater falling in between ($0.81 \pm 0.20 \mu\text{M}$) (Fig. 8). The average phosphate (PO_4^{3-}) concentrations in Jakolof Bay followed the same pattern as ammonium, with the greatest for seawater ($0.62 \pm 0.17 \mu\text{M}$), and the lowest in river water ($0.05 \pm 0.01 \mu\text{M}$), with groundwater falling in between ($0.15 \pm 0.08 \mu\text{M}$) (Fig. 8). The average silicic acid (H_4SiO_4) concentrations in Jakolof Bay were greatest for groundwater and river water ($92.3 \pm 32.9 \mu\text{M}$

Fig. 5 ^{224}Ra versus salinity for all samples taken in Jakolof Bay in autumn 2020, and spring and summer 2021

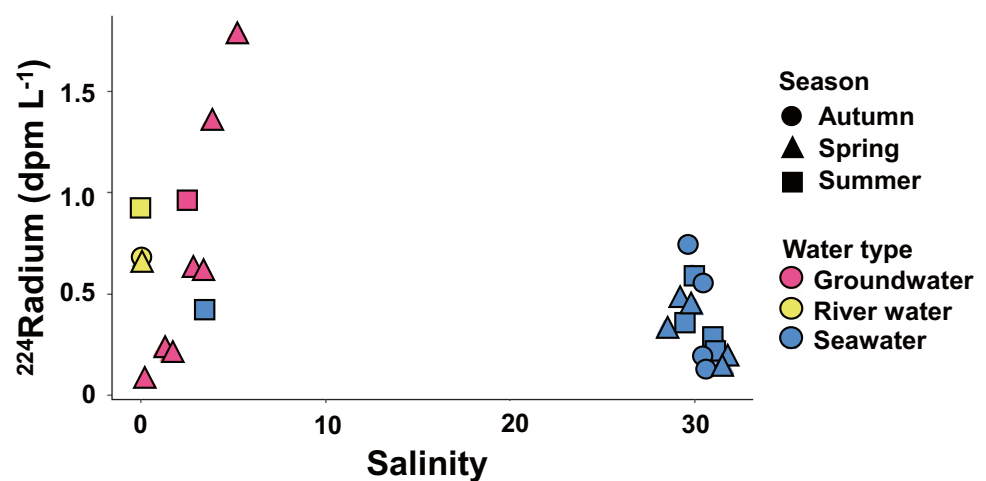
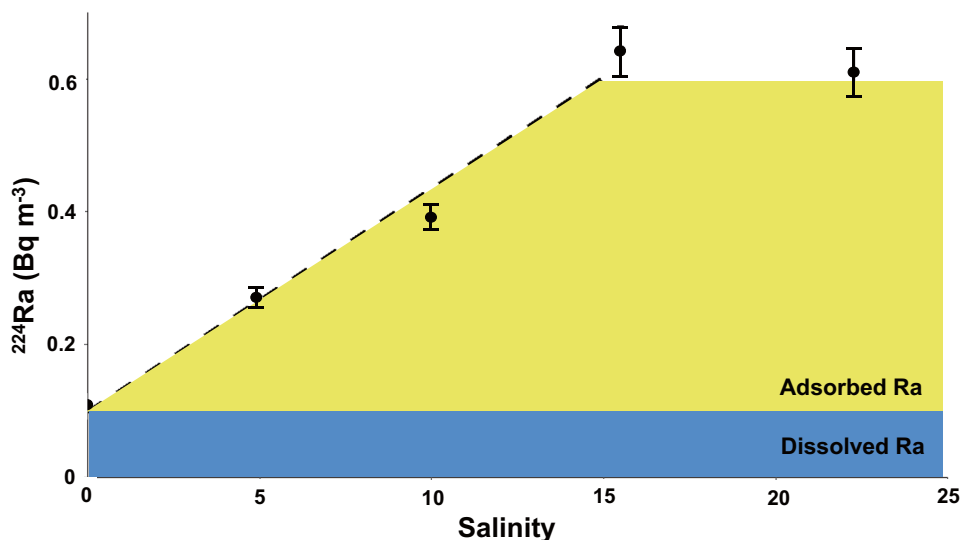


Fig. 6 An experiment using glacial river water and increasing its salinity with NaCl indicates a linear relationship with the desorption of ^{224}Ra activity until a salinity of 15 ($R^2=0.98$). Total desorption of adsorbed Ra is reached at 15 salinity; hence any higher salinity shows the same Ra activity

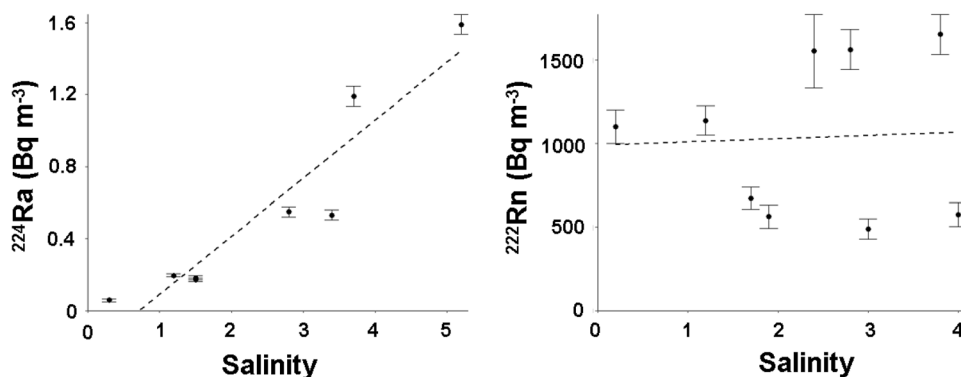


and $92.1 \pm 29.4 \mu\text{M}$, respectively), and lowest in seawater ($15.6 \pm 14.9 \mu\text{M}$) (Fig. 8).

Furthermore, there was greater regeneration of NO_3^- in groundwater in summer than in spring. In spring, the $[\text{NO}_3^-]$ in surface seawater and groundwater were not different (Dunn test, $n=16$, $p\text{-value}=0.285$), thus $[\text{NO}_3^-]$ was not enriched in SGD (Fig. 8). This indicated that organic matter decomposition in sediments yielded no appreciable enhancement of NO_3^- in groundwater and NO_3^- was not removed from seawater. In contrast, groundwater $[\text{NO}_3^-]$ in summer was enriched relative to seawater (Dunn test, $n=9$, $p\text{-value}=0.039$), indicating enrichment of NO_3^- in SGD. In other words, SGD only enriched seawater with NO_3^- in summer and not spring.

Within the Jakolof Bay aquifer system, SGD acted as a sink for PO_4^{3-} . Seawater $[\text{PO}_4^{3-}]$ in spring was lower at low tide compared to high tide but was always considerably higher than groundwater $[\text{PO}_4^{3-}]$, with similar results found in summer (Fig. 8). PO_4^{3-} is highly particle reactive, so it is likely adsorbing to particles within the aquifer and precipitating out of solution. This removal of PO_4^{3-} from recirculating seawater removes the nutrient from the system.

Fig. 7 The activities of ^{224}Ra and ^{222}Rn in groundwater over a range of salinity show a relationship between ^{224}Ra activity and salinity ($R^2=0.86$; left) but there was no relationship between ^{222}Rn activity and salinity ($R^2=-0.14$; right)



Mass Balance Calculations

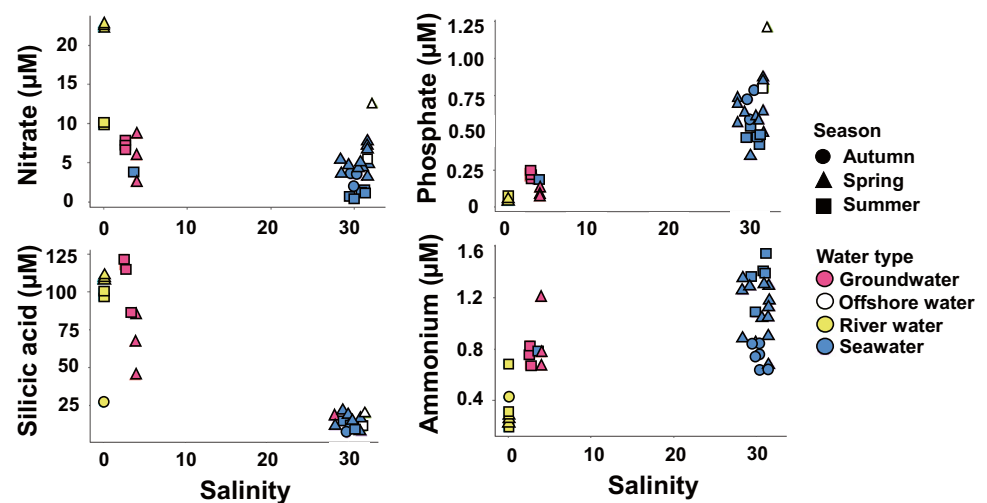
Water Residence Time Estimation

The tidal prism water residence time calculation yielded in water residence time estimates of 0.61 days in September 2020, 0.69 days in May 2021, and 0.69 days in July 2021. The water residence time for the inner half of Jakolof Bay, which encompasses the mudflats (Fig. 1), is 0.24 days in September 2020, 0.30 days in May 2021, and 0.31 days in July 2021. We used the water residence time of the entire bay for the Ra-based SGD as we consider the whole bay in the ^{224}Ra mass balance; however, we used the water residence time of the inner bay for the ^{222}Rn mass balance as it was more representative of the movement of the water at the mooring (Fig. 1).

Radon-Based Total SGD Estimate

The flux estimates used in the ^{222}Rn mass balance from July 2021 data are reported in Table 1. The sediment diffusion flux calculated via lab incubation was found to be

Fig. 8 The concentration of nutrients in the river, groundwater, surface seawater, and depth-integrated offshore waters across three seasons in Jakolof Bay. Offshore water NO_3^- is given as NO_3^- and nitrite. Groundwater samples were taken from a temporary PVC well at ebb tide



$0.29 \text{ Bq m}^{-2} \text{ h}^{-1}$. The offshore loss was estimated to be $91 \text{ Bq m}^{-2} \text{ h}^{-1}$. We estimated F_{mix} a second way by using the tidal prism-based water residence time for inner Jakolof Bay and the ^{222}Rn activity from the timeseries to yield an average offshore mixing estimate of $94 \pm 27 \text{ Bq m}^{-2} \text{ h}^{-1}$, which agrees well with the ^{222}Rn mass balance approach. SGD at low tide ranged from 521 to 689 cm day^{-1} (average = 596 ± 85 , $n = 3$) and at high tide ranged from 0 to 234 cm day^{-1} (average = 97 ± 83 , $n = 8$ (Table 1)). Total SGD is greater at low tide than high tide in Jakolof Bay, and the difference between low and high tide during summer was $500 \pm 119 \text{ cm day}^{-1}$. These results imply that tidal pumping is the dominant control over the rate of SGD.

The total SGD flux in May 2021 was estimated from a mass balance using the difference in the average ^{222}Rn from the surveys at low tide versus high tide. Sediment diffusion was $0.39 \text{ Bq m}^{-2} \text{ h}^{-1}$, mixing loss was $92.4 \text{ Bq m}^{-2} \text{ h}^{-1}$, inventory flux was $475 \text{ Bq m}^{-2} \text{ h}^{-1}$, tidal change was $-27.2 \text{ Bq m}^{-2} \text{ h}^{-1}$, atmospheric evasion was $4.08 \text{ Bq m}^{-2} \text{ h}^{-1}$, and the river

flux term was $1.21 \text{ Bq m}^{-2} \text{ h}^{-1}$, resulting in a total SGD of 241 cm day^{-1} . Comparing with the summer value of $233 \pm 245 \text{ cm day}^{-1}$ suggests that there is no seasonal difference in total SGD, further indicating that the tidal stage is the dominant driver of SGD variability throughout the year.

Radium-Based Total SGD Estimate

The flux estimates used in the ^{224}Ra mass balance in autumn 2020, spring 2021, and summer 2021 are reported in Table 2. From greatest to least, the average activity of ^{224}Ra in Jakolof Bay seawater in autumn 2020 was $0.45 \pm 0.07 \text{ Bq m}^3$, in summer 2021 was $0.38 \pm 0.05 \text{ Bq m}^3$, in spring 2021 at low tide was $0.30 \pm 0.04 \text{ Bq m}^3$, and in spring 2021 at high tide was $0.21 \pm 0.03 \text{ Bq m}^3$. The ^{224}Ra -based SGD estimates were $15.4 \pm 3.4 \text{ m}^3 \text{ s}^{-1}$ in autumn 2020, $0.7 \pm 1.2 \text{ m}^3 \text{ s}^{-1}$ at high tide and $6.1 \pm 1.5 \text{ m}^3 \text{ s}^{-1}$ at low tide in spring 2021, and $5.9 \pm 0.8 \text{ m}^3 \text{ s}^{-1}$ in summer 2021, for an average

Table 1 The inventory flux, tidal change, and atmospheric evasion estimated for the ^{222}Rn mass balance to solve for total SGD. The sediment diffusion flux and mixing loss flux were $0.29 \text{ Bq m}^{-2} \text{ h}^{-1}$ and $91.27 \text{ Bq m}^{-2} \text{ h}^{-1}$, respectively, for each timestep

Time (HH:MM)	Inventory flux ($\text{Bq m}^{-2} \text{ h}^{-1}$)	Tidal change ($\text{Bq m}^{-2} \text{ h}^{-1}$)	Atmospheric evasion ($\text{Bq m}^{-2} \text{ h}^{-1}$)	Total SGD (cm day^{-1})
7:45 to 8:45	445.45	-5.21	0.89	689
8:45 to 9:45	-42.82	-2.18	0.82	61
9:45 to 10:45	-32.91	18.75	3.02	104
10:45 to 11:45	-167.92	70.76	6.18	0
11:45 to 12:45	-35.75	118.30	6.92	234
12:45 to 13:45	-162.36	118.68	11.19	76
13:45 to 14:45	-86.20	86.20	14.01	136
14:45 to 15:45	-31.13	46.41	14.43	156
15:45 to 16:45	-94.44	1.02	9.14	9
16:45 to 17:45	289.92	-2.90	23.84	521
17:45 to 18:45	334.08	-6.53	28.29	579

Table 2 The offshore mixing, ^{224}Ra decay, river input, and sediment diffusion fluxes estimated for the ^{224}Ra mass balance to solve for total SGD

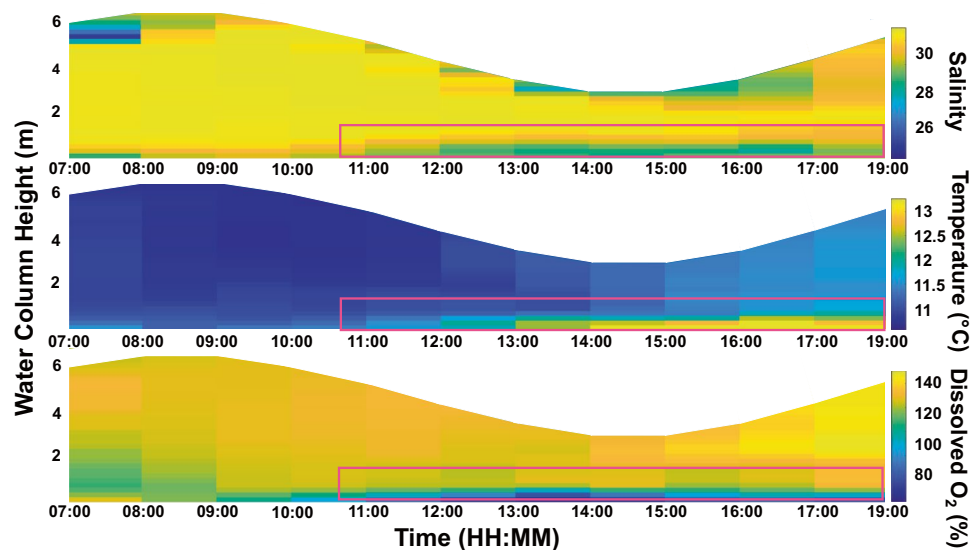
Season	Offshore mixing (Bq s ⁻¹)	^{224}Ra decay (Bq s ⁻¹)	River input (Bq s ⁻¹)	Sediment diffusion (Bq s ⁻¹)	Total SGD (m ³ s ⁻¹)
Autumn 2020	8.7 ± 0.6	6.2 ± 1.0	2.1 ± 0.2	0.1 ± 0.1	15.4 ± 3.3
Spring 2021, low tide	2.4 ± 0.5	2.5 ± 0.3	0.7 ± 0.1	0.1 ± 0.1	6.1 ± 1.5
Spring 2021, high tide	-2.6 ± 0.6	3.8 ± 0.6	0.7 ± 0.1	0.1 ± 0.1	0.7 ± 1.2
Summer 2021	2.8 ± 0.6	3.4 ± 0.5	0.5 ± 0.1	0.1 ± 0.1	5.9 ± 0.8

of $7.0 \pm 12.5 \text{ m}^3 \text{ s}^{-1}$. To compare these values to the ^{222}Rn -based SGD estimates, we divided the Ra-based estimates by the seepage face (i.e., the area of seafloor in m² where SGD is free to exit from the subsurface). This conversion of the averaged Ra-based SGD estimate resulted in an SGD flux of $86 \pm 154 \text{ cm day}^{-1}$, which is an order of magnitude lower than the ^{222}Rn -based SGD estimates (241 cm day^{-1} in spring and $233 \pm 245 \text{ cm day}^{-1}$ in summer).

Fresh SGD Estimates

In Jakolof Bay, hourly CTD profiles taken on July 17, 2021, over a tidal cycle revealed a direct observation of SGD (Fig. 9). Specifically, we observed a layer of relatively warm, brackish, and oxygen-poor water directly above the seafloor. The magnitude of this fresher signal indicated that fresh/brackish SGD constituted a substantial fraction of the total SGD signal. The fresh SGD estimates from July using the mass balance approach resulted in values ranging from 18 to 39 cm day⁻¹ ($24 \pm 8 \text{ cm day}^{-1}$, $n = 12$) over the tidal cycle. Therefore, the percent of fresh SGD in summer is 11% of the ^{222}Rn -based total SGD estimates. The fresh SGD estimate using the well salinity method in spring resulted in a value of $73 \pm 6 \text{ cm day}^{-1}$, which accounted for 30% of the ^{222}Rn -based total SGD estimates.

Fig. 9 Water column salinity (top), temperature (middle), and dissolved oxygen (bottom) in Jakolof Bay on July 17th, 2021, during the 12-h zodiac mooring. Highlighted by the box is a relatively fresh, warm, and oxygen-poor layer presumed to be an SGD signal



Sources of Nutrients to Jakolof Bay

SGD and offshore mixing were the dominant sources of NO_3^- in Jakolof Bay, with offshore mixing providing the greatest supply in May while SGD provided the greatest supply in July (Table 3). Our results also indicated that SGD provided a greater flux of NH_4^+ to Jakolof Bay than river water (Table 3); though a comparison to offshore water could not be made as offshore NH_4^+ was not measured. In both spring and summer, offshore mixing was the greatest source of PO_4^{3-} and SGD was the greatest source of H_4SiO_4 (Table 3). Indeed, consistent linear declines in seawater $[\text{H}_4\text{SiO}_4]$ with distance from the mudflats ($R^2 = 0.89$ in spring at low tide, and $R^2 = 0.87$ in summer) implied a source at the bay's head.

There was a linear increase in N:P ($\text{NO}_3^- / \text{PO}_4^{3-}$) with distance from the mudflats (Fig. 10), indicating mixing with higher N:P offshore waters. Linear correlations were observed between N:P and distance from the head of the bay in September 2020 ($R^2 = 0.83$), in May at low and high tide ($R^2 = 0.49$ and $R^2 = 0.78$, respectively), and in July 2021 ($R^2 = 0.75$). The lower N:P at the head of the bay (< 10) did not appear to be explained from the input of groundwater nor river water whose N:P ranged from 63.43 in May to 34.09 in July, and 145.2 in September to 615.2 in May, respectively.

Table 3 Nutrient inputs to Jakolof Bay in spring and summer 2021

Source	Water discharge (m ³ s ⁻¹)	NO ₃ ⁻ flux (mmol day ⁻¹)	NH ₄ ⁺ flux (mmol day ⁻¹)	PO ₄ ³⁻ flux (mmol day ⁻¹)	H ₄ SiO ₄ flux (mmol day ⁻¹)
May 2021					
River	1.1	2.1 ± 0.2	0.023 ± 0.0029	0.004 ± 0.002	9.8 ± 0.9
²²² Rn-based SGD	20 ± 7	9.4 ± 9.0	1.5 ± 1.0	0.15 ± 0.13	110 ± 92
Offshore mixing	24 ± 2	26 ± 12	-	2.5 ± 1.1	40 ± 18
July 2021					
River	0.6	0.52 ± 0.04	0.0012 ± 0.0008	0.003 ± 0.001	5.2 ± 0.6
²²² Rn-based SGD, low tide	49 ± 7	32 ± 15	3.2 ± 1.3	0.93 ± 0.45	510 ± 200
²²² Rn-based SGD, high tide	8 ± 6	5.1 ± 4.9	0.51 ± 0.45	0.15 ± 0.14	82 ± 75
Offshore mixing	24 ± 2	11 ± 5.0	-	1.7 ± 0.75	23 ± 10

Discussion

Submarine groundwater discharge (SGD) was a major contributor of NO₃⁻ and H₄SiO₄ to Jakolof Bay, Alaska, while offshore mixing provided the majority of the PO₄³⁻ (Table 3). Offshore water, originating as part of the Alaska Coastal Current (ACC), a buoyancy-driven coastal current that enters Jakolof Bay following bathymetric contours (Stabeno et al. 2004; Field and Walker 2003), is typically nutrient-rich (Childers et al. 2005). Sambrotto and Lorenzen (1986) suggested that the water outside the mouth of Jakolof Bay is one of the most biologically productive ecosystems in the world due to the high supply of nutrients to surface waters from frequent storms and persistent currents stimulating strong, vertical mixing along the continental shelf. Estimates of nutrient discharge from SGD at a nearby rocky beach suggest that groundwater plays a larger role in the input of nutrients to the nearshore than rivers (Lecher et al. 2016b). This study confirmed the importance of SGD as a source of macronutrients and compared it to offshore water.

Comparisons to Other Locations

Groundwater Endmembers

The ²²²Rn groundwater endmembers used in this study compared well with those reported by Dulai et al. (2016) in a wetland in Kaneohe Bay, Hawaii (1500 ± 1300 Bq m⁻³), Wu et al. (2013) in the East China Sea (1710 to 1739 Bq m⁻³), and Burnett and Dulaiova (2003) using incubations of nearshore sediment in the Gulf of Mexico (2170 ± 730 Bq m⁻³). In contrast, lower groundwater ²²²Rn activity was measured using similar temporary PVC wells at the beach face at Kasitsna Bay (702 ± 103 Bq m⁻³, Dimova et al. 2015), a second rocky beach < 25 km from Jakolof Bay near the Grewingk River (59.6417, -151.1940) (366 ± 19 Bq m⁻³), and at an Alaskan lake (400 ± 8.3 Bq m⁻³, Dabrowski et al. 2020).

The ²²⁴Ra groundwater endmember used for spring (0.61 ± 0.12, *n* = 7), summer (0.84 ± 0.04 Bq m⁻³), and autumn (0.73 ± 0.15 Bq m⁻³) were within the low end

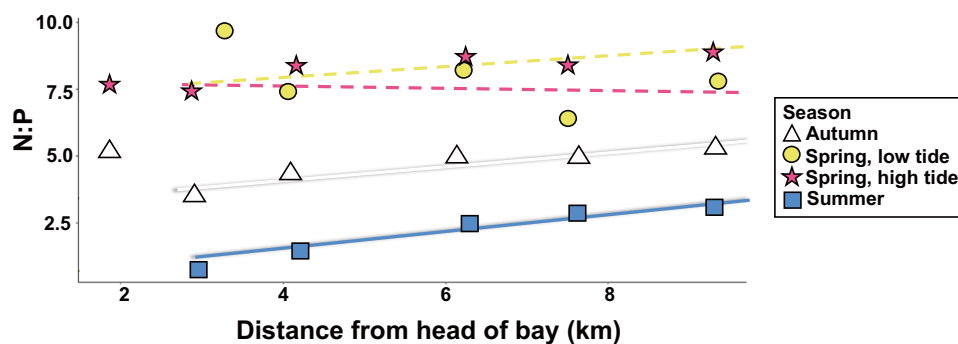


Fig. 10 The correlation between N:P and distance from the head of the bay. The N:P value reflects the ratio of NO₃⁻/PO₄³⁻. The linear regression is fitted with a solid line when *p*-value < 0.05 and a dashed line when *p*-value > 0.05. The linear regressions fit to the N:P data

from autumn ($R^2=0.83$), spring low tide ($R^2=0.49$), spring high tide ($R^2=0.78$), and summer ($R^2=0.75$) did not include the first data point. The first data point in summer is 20.09, and above the *y*-axis limits for the graph therefore not displayed

of the range reported at the rocky beach of Kasitsna Bay (0.445 to 5.40 Bq m⁻³, Lecher et al. 2016a). They were much lower than Bega River estuary, Australia (199 Bq m⁻³ to 683 Bq m⁻³; Hancock et al. 2000), Jiaozhou Bay, China (258 Bq m⁻³; Zhang et al. 2020), and the north side of Kachemak Bay (59.6385 , -151.4800) which is < 15 km from Jakolof Bay (9.97 ± 0.53 Bq m⁻³).

Estimates of SGD

Similar ²²²Rn-based SGD estimates were observed between our mudflat site and a nearby rocky beach in the NGA. The SGD in the Jakolof Bay mudflat in summer 2021 ranged across the tidal cycle from 0 to 689 cm day⁻¹ (233 ± 245 cm day⁻¹, $n = 10$) and at the rocky beach of Kasitsna Bay it averaged 260 ± 360 cm day⁻¹ ($n = 149$) in 2011 and 130 ± 180 cm day⁻¹ ($n = 145$) in 2012 (Dimova et al. 2015). Though the mudflat contains less permeable sediment than the rocky beach, these results indicate that SGD across two disparate substrates are in the same order of magnitude, supporting the extrapolation of SGD-associated nutrient discharge to the entire NGA as done by Lecher et al. (2016b). The similarity between SGD values in such different settings demonstrates the importance of tidal pumping as a driver.

The discrepancy between the ²²²Rn- and ²²⁴Ra-based estimates is likely due to the tracers' sensitivity to different processes. As suggested by Lecher et al. (2016a), ²²²Rn accounts for both the fresh and saline components of SGD, while ²²⁴Ra may capture brackish to saline SGD. The desorption experiment conducted at Grewingk River (Fig. 6) showed that 83% more ²²⁴Ra desorbed from suspended particles at a salinity greater than 20. Any fresh SGD passing through the aquifer in Jakolof likely contained a lower ²²⁴Ra activity (Fig. 7), so the ²²⁴Ra mass balance only captured the elevated salinity SGD. However, the difference between the two tracers may also be a result of overestimating the seepage face which makes the conversion between the two methods difficult. Further work would be needed to identify the true seepage face, as well as any heterogeneity in SGD across this interface.

Nevertheless, the flux of SGD appears greater in the NGA than the global average (Santos et al. 2021). Globally, saline SGD dominates total SGD by $> 99\%$ relative to fresh SGD (Santos et al. 2021; Kwon et al. 2014) and the tidal range in this region of southcentral Alaska—the primary mechanism driving saline SGD—is among the largest on the planet (Archer 2013). This resulted in estimates of total SGD in the NGA one to three orders of magnitude greater than the median SGD rates reported in both the Pacific (2 – 22 cm day⁻¹) and Atlantic Oceans (1 – 10 cm day⁻¹) (Santos et al. 2021). However, not all regions of the NGA are characterized by up to 8 m tidal ranges; therefore, repeating a similar study as this one in locations with smaller tidal ranges are needed to support the claim from

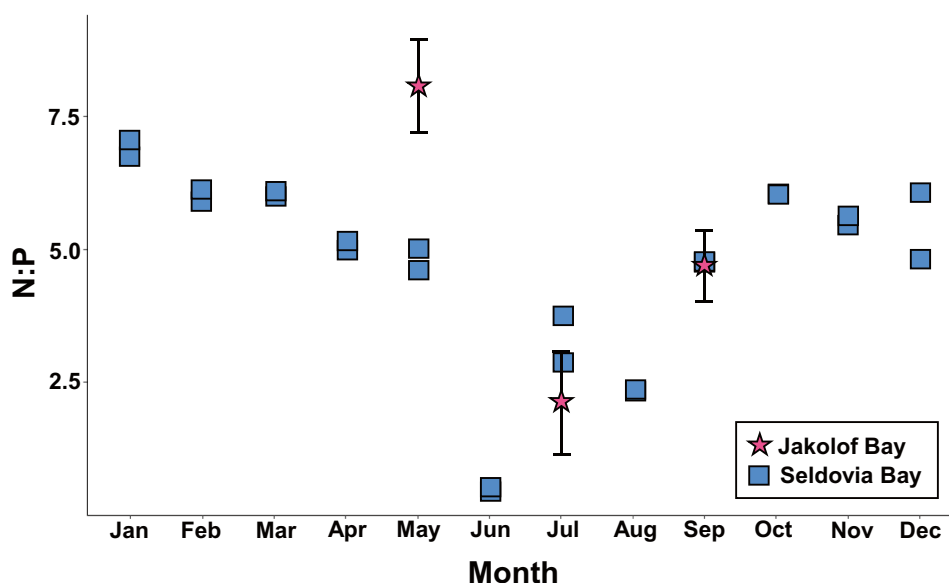
Lecher et al. (2016b) that SGD rivals river discharge as a source of macronutrients in the NGA.

While global total SGD is $< 1\%$ fresh (Santos et al. 2021; Taniguchi et al. 2008) and this study estimated fresh SGD accounting for 11 to 30% of the total flux, Wang et al. (2015) also measured a fresh to saline SGD ratio as ranging from 7 to 8.2% in Laizhou Bay, China. The fresh SGD estimates from Jakolof Bay were 3 orders of magnitude greater than the nearby rocky beach at Kasitsna Bay (Dimova et al. 2015). For comparison, Dimova et al. (2015) calculated that fresh SGD was 1% of the total SGD flux. In that study, the seawater had a salinity of 31.2 and assuming a fresh SGD salinity of 0, the total SGD would have a salinity of 30.1. In contrast, the minimum salinity recorded above the seafloor in Jakolof Bay was 25 (Fig. 8), suggesting that the fresh SGD at the mudflat in Jakolof Bay made up a much larger fraction of total SGD than the rocky beach at Kasitsna Bay. This supports the difference seen between the ²²⁴Ra-based SGD estimate (saline SGD) versus the ²²²Rn-based SGD estimate (saline and fresh SGD).

Short Aquifer Water Residence Time

The relatively high groundwater [NO_3^-] suggested a short residence time in the Jakolof Bay aquifer (Fig. 8). In deep aquifers with long residence times, dissolved oxygen is often consumed entirely, leading to declines in porewater [NO_3^-] via denitrification (Slomp and Cappellen 2004; Hunter et al. 1998). Since the [NO_3^-] was high in the fresh groundwater of Jakolof Bay (5.50 ± 3.02 μM in salinity 3.9 in spring and 7.50 ± 0.68 μM in salinity 0.1 in summer) (Fig. 8), it indicated that denitrification had not yet occurred to reduce groundwater NO_3^- and therefore the groundwater was not oxygen-limited. Indeed, pore water timeseries data collected by Miller and Kelley (2021a) throughout June 2019 in Jakolof Bay yielded porewater oxygen concentrations in the top 10 cm of the sediment between 94 and 562 μM (average = 330 ± 87 , $n = 67$). The aquifer water residence times were found to be short in Kasitsna Bay as well due to elevated [NO_3^-] and water isotopes falling on the Global Meteoric Water Line (Lecher et al. 2016a, b). Further proof of the oxic nature of the aquifer in Jakolof Bay is the low [NH_4^+] relative to [NO_3^-]. If the groundwater is well oxygenated, as appears to be the case in Jakolof Bay, NH_4^+ becomes readily oxidized to NO_3^- (Santos et al. 2021; Charette and Buesseler 2004). As the [NO_3^-] is an order of magnitude greater than the [NH_4^+] in Jakolof Bay groundwater, which is seen with the Kasitsna Bay aquifer as well (Lecher et al. 2016b), it suggests that the nitrogen cycle is simplified in the Jakolof Bay aquifer and that there is little NO_3^- attenuation. All the evidence that the Jakolof Bay aquifer was oxic therefore suggests that the aquifer water residence time was short.

Fig. 11 The N:P in Seldovia Bay decreases from winter to late summer in 2019, before increasing in autumn. The three spot samples taken in Jakolof Bay from 2021 and offshore water reported in Childers et al. (2005) follow the same trend. The N:P indicates the ratio of $\text{NO}_3^-/\text{PO}_4^{3-}$



N:P Dynamics

The ratio of NO_3^- to PO_4^{3-} is used to identify the limiting nutrient in seawater, assuming the general requirement for phytoplankton loosely follows the Redfield ratio (N:P=16). The N:P in Jakolof Bay seawater was < 10 throughout the year, implying that NO_3^- was the major limiting nutrient (Fig. 10). The decrease in seawater [NO_3^-] from spring to autumn (Dunn test, p -value = 3.11) was likely due to producers using up the nutrients in summer and autumn. Similar N:P ratios are reported in nearby Seldovia Bay (Fig. 11) and in offshore (NGA) waters (Childers et al. 2005). The dominant sources of the limiting nutrient in Jakolof Bay, NO_3^- , shifted from spring to summer. While the SGD NO_3^- flux increased from spring to summer ($9.4 \pm 9.0 \text{ mmol day}^{-1}$ and $19 \pm 16 \text{ mmol day}^{-1}$, respectively), the NO_3^- flux from offshore mixing was reduced by half ($26 \pm 12 \text{ mmol day}^{-1}$ and $11 \pm 5 \text{ mmol day}^{-1}$, respectively) (Table 2), shifting the dominant source of NO_3^- from offshore mixing of NGA water to SGD from spring to summer.

Furthermore, our data cannot explain the low N:P ratio at the head of Jakolof Bay (Fig. 10). It is not due to biological uptake or regeneration in the water column as that does not change the N:P. Denitrification, the removal of biologically available nitrogen, was unlikely to occur in oxic, well-mixed seawater. Though the following are the typical explanations for low N:P in coastal water, (1) the oxic conditions in the Jakolof Bay sediment (Miller and Kelly 2021a) cannot induce faster regeneration of PO_4^{3-} relative to NO_3^- in sediment (Nixon 1980, 1981), and (2) the desorption of PO_4^{3-} from iron- and manganese-(hydr) oxides during reducing conditions in the sediment (Nixon 1980, 1981) is unlikely due to the aquifer acting as a sink for PO_4^{3-} . However, the N:P could be lowered at the head of the bay

due to additional PO_4^{3-} desorbing from riverine suspended solids or resuspended bottom sediment at the head of the bay stirred up as river discharge flowed past.

As a particle-reactive species, over 90% of the total PO_4^{3-} discharged by rivers is associated with suspended solids. Desorption occurs in seawater because (1) surface seawater has low [PO_4^{3-}] compared to rivers, and (2) anions competing for surface binding sites on suspended solids with PO_4^{3-} are all orders of magnitude greater in seawater than freshwater (Froelich 1988). From our river ^{224}Ra desorption experiment, the ratio of ^{224}Ra adsorbed to riverine suspended solids to dissolved ^{224}Ra was 15:1 (Fig. 6) showing a large, potential input of desorbing elements from suspended solids. Similarly, Froelich (1988) describes 2- to fivefold more PO_4^{3-} desorbs from riverine suspended solids than is dissolved in river water, making the desorbable fraction of PO_4^{3-} from riverine suspended solids a large input into coastal waters. To summarize, while our results indicated that river discharge was not a large source of dissolved PO_4^{3-} , we were perhaps missing a critical contribution of PO_4^{3-} from riverine suspended solids.

Conclusions

The large tidal range in the NGA plays a vital role in maintaining the high nutrient-supply in nearshore systems. The huge tidal prism results in the residence times in Jakolof Bay being less than 1 day, and tidal pumping drives high fluxes of groundwater. Both SGD and offshore mixing are dominant sources of macronutrients to the nearshore. Additionally, independent calculations of SGD from radon and radium tracers resulted in estimates an order of magnitude apart. However, taking more groundwater samples in the future

will help further constrain that endmember. The SGD values compared well with estimates from a rocky beach within the region, suggesting that the flux of SGD may be large across the entire NGA coastline regardless of substrate type. SGD and offshore mixing, though difficult to measure, should be taken into account when studying nearshore biogeochemical cycles in the NGA. Further research would benefit from investigating the flux of SGD in regions of the NGA with a smaller tidal range and the fraction of PO_4^{3-} associated with suspended solids discharged from rivers.

Acknowledgements This paper was written at the University of Alaska Troth Yeddha' campus on the unceded traditional homelands of the Lower Tanana Dené. This research was conducted as a guest working on the unceded traditional homelands of the Dena'ina and Alutiiq peoples.

The authors thank Dr. Ana Aguilar-Islas, Dr. Amanda Kelley, Dr. Mark Johnson, Dr. LeeAnn Munk, Emily Ortega, Marina Alcantar, Shelby Bacus, James Currie, Jonah Jossart, Aeon Russo, and Feyne Elmore. The authors are grateful to the staff of the Kasitsna Bay Laboratory. The author and this research were financially supported by the University of Alaska Coastal Marine Institute in partnership with the Bureau of Ocean Energy Management Alaska OCS Region under cooperative agreement M20AC10016, and the Alaska Established Program to Stimulate Competitive Research National Science Foundation award #OIA-1757348 and the state of Alaska. The authors thank the Northern Gulf of Alaska Long Term Ecological Reserve and the NOAA National Estuarine Research Reserve System for use of their data.

Open Access This article is licensed under a Creative Commons Attribution 4.0 International License, which permits use, sharing, adaptation, distribution and reproduction in any medium or format, as long as you give appropriate credit to the original author(s) and the source, provide a link to the Creative Commons licence, and indicate if changes were made. The images or other third party material in this article are included in the article's Creative Commons licence, unless indicated otherwise in a credit line to the material. If material is not included in the article's Creative Commons licence and your intended use is not permitted by statutory regulation or exceeds the permitted use, you will need to obtain permission directly from the copyright holder. To view a copy of this licence, visit <http://creativecommons.org/licenses/by/4.0/>.

References

- Archer, A.W. 2013. World's highest tides: Hypertidal coastal systems in North America, South America and Europe. *Sedimentary Geology* 284: 1–25.
- Armstrong, F.A.J., C.R. Stearns, and J.D.H. Strickland. 1967. The measurement of upwelling and subsequent biological processes by means of the Technicon Autoanalyzer and associated equipment. *Deep-Sea Research* 14: 381–389.
- Burnett, W.C., and H. Dulaiova. 2003. Estimating the dynamics of groundwater input into the coastal zone via continuous radon-222 measurements. *Journal of Environmental Radioactivity* 69 (1–2): 21–35.
- Burnett, W.C., R. Peterson, W.S. Moore, and J. de Oliveira. 2008. Radon and radium isotopes as tracers of submarine groundwater discharge—results from the Ubatuba, Brazil SGD assessment intercomparison. *Estuarine, Coastal and Shelf Science* 76 (3): 501–511.
- Charette, M.A., and K.O. Buesseler. 2004. Submarine groundwater discharge of nutrients and copper to an urban subestuary of Chesapeake Bay (Elizabeth River). *Limnology and Oceanography* 49 (2): 376–385.
- Childers, A.R., T.E. Whitledge, and D.A. Stockwell. 2005. Seasonal and interannual variability in the distribution of nutrients and chlorophyll a across the Gulf of Alaska shelf: 1998–2000. *Deep Sea Research Part II: Topical Studies in Oceanography* 52 (1–2): 193–216.
- Corbett, D.R., W.C. Burnett, P.H. Cable, and S.B. Clark. 1997. Radon tracing of groundwater input into Par Pond, Savannah River site. *Journal of Hydrology* 203 (1–4): 209–227.
- Crotwell, A.M., and W.S. Moore. 2003. Nutrient and radium fluxes from submarine groundwater discharge to Port Royal Sound. *South Carolina. Aquatic Geochemistry* 9 (3): 191–208.
- Dabrowski, J.S., M.A. Charette, P.J. Mann, S.M. Ludwig, S.M. Natali, R.M. Holmes, J.D. Schade, M. Powell, and P.B. Henderson. 2020. Using radon to quantify groundwater discharge and methane fluxes to a shallow, tundra lake on the Yukon-Kuskokwim Delta. *Alaska. Biogeochemistry* 148 (1): 69–89.
- Dimova, N.T., A. Paytan, J.D. Kessler, K.J. Sparrow, F. Garcia-Tigreros Kodovska, A.L. Lecher, J. Murray, and S.M. Tulaczyk. 2015. Current magnitude and mechanisms of groundwater discharge in the Arctic: Case study from Alaska. *Environmental Science & Technology* 49 (20): 12036–12043.
- Dulai, H., A. Kleven, K. Ruttenberg, R. Briggs, and F. Thomas. 2016. Evaluation of submarine groundwater discharge as a coastal nutrient source and its role in coastal groundwater quality and quantity. In *Emerging issues in groundwater resources*, ed. A. Fares, 187–221. Cham: Springer.
- Erőss, A., J. Mádl-Szőnyi, H. Surbeck, Á. Horváth, N. Goldscheider, and A.É. Csoma. 2012. Radionuclides as natural tracers for the characterization of fluids in regional discharge areas, Buda Thermal Karst, Hungary. *Journal of Hydrology* 426: 124–137.
- Field, C.M., and C. Walker. 2003. A site profile of the Kachemak Bay Research Reserve, a unit of the National Estuarine Research Reserve System. Kachemak Bay Research Reserve.
- Froelich, P.N. 1988. Kinetic control of dissolved phosphate in natural rivers and estuaries: A primer on the phosphate buffer mechanism 1. *Limnology and Oceanography* 33: 649–668.
- Garcia-Orellana, J., V. Rodellas, J. Tamborski, M. Diego-Feliu, P. van Beek, Y. Weinstein, M. Charette, A. Alorda-Kleinglass, H.A. Michael, T. Stieglitz, and J. Scholten. 2021. Radium isotopes as submarine groundwater discharge (SGD) tracers: review and recommendations. *Earth-Science Reviews* 103681.
- Garcia-Solsona, E., J. Garcia-Orellana, P. Masqué, and H. Dulaiova. 2008. Uncertainties associated with ^{223}Ra and ^{224}Ra measurements in water via a Delayed Coincidence Counter (RaDeCC). *Marine Chemistry* 109 (3–4): 198–219.
- Hancock, G.J., I.T. Webster, P.W. Ford, and W.S. Moore. 2000. Using Ra isotopes to examine transport processes controlling benthic fluxes into a shallow estuarine lagoon. *Geochimica Et Cosmochimica Acta* 64 (21): 3685–3699.
- Happell, J.D., J.P. Chanton, G.J. Whiting, and W.J. Showers. 1993. Stable isotopes as tracers of methane dynamics in Everglades marshes with and without active populations of methane oxidizing bacteria. *Journal of Geophysical Research: Atmospheres* 98 (D8): 14771–14782.
- Hartwell, S. I., D. Dasher, and T. Lomax. 2016. Characterization of benthic habitats and contaminant assessment in Kenai Peninsula fjords and bays, NOAA Technical Memorandum NOS NCCOS. <https://repository.library.noaa.gov/view/noaa/16234>. Accessed 24 March 2022.
- Hunter, K.S., Y. Wang, and P. Van Cappellen. 1998. Kinetic modeling of microbially-driven redox chemistry of subsurface environments: Coupling transport, microbial metabolism and geochemistry. *Journal of Hydrology* 209 (1–4): 53–80.

- Jenckes, J., L. Munk, D. Ibarra, D. Boutt, J. Fellman, & E. Hood. 2023. Hydroclimate Drives Seasonal Riverine Export Across a Gradient of Glacierized High-Latitude Coastal Catchments. *Water Resources Research* 59(4).
- Kerouel, R., and A. Aminot. 1997. Fluorometric determination of ammonia in sea and estuarine waters by direct segmented flow analysis. *Marine Chemistry* 57 (3–4): 265–275.
- Kim, G., K.K. Lee, K.S. Park, D.W. Hwang, and H.S. Yang. 2003. Large submarine groundwater discharge (SGD) from a volcanic island. *Geophysical Research Letters* 30(21).
- Krest, J.M., W.S. Moore, L.R. Gardner, and J.T. Morris. 2000. Marsh nutrient export supplied by groundwater discharge: Evidence from radium measurements. *Global Biogeochemical Cycles* 14 (1): 167–176.
- Kwon, E.Y., G. Kim, F. Primeau, W.S. Moore, H.M. Cho, T. DeVries, J.L. Sarmiento, M.A. Charette, and Y.K. Cho. 2014. Global estimate of submarine groundwater discharge based on an observationally constrained radium isotope model. *Geophysical Research Letters* 41 (23): 8438–8444.
- Lecher, A.L., C.T. Chien, and A. Paytan. 2016b. Submarine groundwater discharge as a source of nutrients to the North Pacific and Arctic coastal ocean. *Marine Chemistry* 186: 167–177.
- Lecher, A.L., J. Kessler, K. Sparrow, F. Garcia-Tiguerros Kodovska, N. Dimova, J. Murray, S. Tulaczyk, and A. Paytan. 2016a. Methane transport through submarine groundwater discharge to the North Pacific and Arctic Ocean at two Alaskan sites. *Limnology and Oceanography* 61 (S1): S344–S355.
- Lecher, A.L., K.R. Mackey, and A. Paytan. 2017. River and submarine groundwater discharge effects on diatom phytoplankton abundance in the Gulf of Alaska. *Hydrology* 4 (4): 61.
- MacIntyre, S., R. Wannikhof, and J.P. Chanton. 1995. Trace gas exchange across the air-water interface in freshwater and coastal marine environments. In *Biogenic trace gases: measuring emissions from soil and water*, ed. P.A. Matson and R.C. Hariss, 52–57. Backwell Science.
- Miller, C.A., and A.L. Kelley. 2021a. Alkalinity cycling and carbonate chemistry decoupling in seagrass mystify processes of acidification mitigation. *Scientific Reports* 11 (1): 1–12.
- Miller, C.A., and A.L. Kelley. 2021b. Seasonality and biological forcing modify the diel frequency of nearshore pH extremes in a subarctic Alaskan estuary. *Limnology and Oceanography* 66 (4): 1475–1491.
- Moore, W.S. 2003. Sources and fluxes of submarine groundwater discharge delineated by radium isotopes. *Biogeochemistry* 66 (1): 75–93.
- Murphy, J., and J.P. Riley. 1962. A modified single solution method for the determination of phosphate in natural waters. *Analytica Chimica Acta* 27: 31–36.
- Niencheski, L.F.H., H.L. Windom, W.S. Moore, and R.A. Jahnke. 2007. Submarine groundwater discharge of nutrients to the ocean along a coastal lagoon barrier. *Southern Brazil. Marine Chemistry* 106 (3–4): 546–561.
- Nixon, S.W. 1980. Between coastal marshes and coastal waters—a review of twenty years of speculation and research on the role of salt marshes in estuarine productivity and water chemistry. *Estuarine and Wetland Processes* 1980: 437–525.
- Nixon, S.W. 1981. Remineralization and nutrient cycling in coastal marine ecosystems. In *Estuaries and Nutrients*, ed. B.J. Neilson and L.E. Cronin, 111–138. Humana Press.
- NOAA National Estuarine Research Reserve System (NERRS). System-wide monitoring program. Data accessed from the NOAA NERRS Centralized Data Management Office website: <http://www.nerrsdata.org>. Accessed 16 November 2021.
- NOAA National Weather Service Hydrogeological Design Studies Center. Data accessed from the NOAA Precipitation Frequency Data Server (PFDS). <https://hdsc.nws.noaa.gov/hdsc/pfds/>. Accessed 10 Mar 2023.
- R Core Team. 2022. R: a language and environment for statistical computing. R Foundation for Statistical Computing, Vienna, Austria. <https://www.R-project.org/>.
- Rodellas, V., J. Garcia-Orellana, P. Masqué, M. Feldman, and Y. Weinstein. 2015. Submarine groundwater discharge as a major source of nutrients to the Mediterranean Sea. *Proceedings of the National Academy of Sciences* 112 (13): 3926–3930.
- Sambrotto, R.N. and C.J. Lorenzen. 1986. Phytoplankton and primary productivity. In *The Gulf of Alaska Physical Environment and Biological Resources*, ed. D.W. Hood and S.T. Zimmerman, 249–282. OCS Study 86–0095 USDOC, NOAA, NOS, and USDOI, MMS, Alaska OCS Region. Anchorage, AK.
- Santos, I.R., X. Chen, A.L. Lecher, A.H. Sawyer, N. Moosdorf, V. Rodellas, J. Tamborski, H.M. Cho, N. Dimova, R. Sugimoto, S. Bonaglia, H. Li, M. Hajati, and L. Li. 2021. Submarine groundwater discharge impacts on coastal nutrient biogeochemistry. *Nature Reviews Earth & Environment* 2 (5): 307–323.
- Schmoll, H.R., L.A. Yehle, C.A. Gardner, and J.K. Odum. 1984. Guide to surficial geology and glacial stratigraphy in the upper Cook Inlet basin. Geological Society of America, Cordilleran Section. https://ngmdb.usgs.gov/Prodesc/proddesc_89397.htm. Accessed 27 Feb 2021.
- Slopp, C.P., and P. Van Cappellen. 2004. Nutrient inputs to the coastal ocean through submarine groundwater discharge: Controls and potential impact. *Journal of Hydrology* 295 (1–4): 64–86.
- Stabeno, P.J., N.A. Bond, A.J. Hermann, N.B. Kachel, C.W. Mordy, and J.E. Overland. 2004. Meteorology and oceanography of the Northern Gulf of Alaska. *Continental Shelf Research* 24 (7–8): 859–897.
- Taniguchi, M., W.C. Burnett, H. Dulaiova, F. Siringan, J. Foronda, G. Wattayakorn, S. Rungsupa, E.A. Kontar, and T. Ishitobi. 2008. Groundwater discharge as an important land-sea pathway into Manila Bay, Philippines. *Journal of Coastal Research* 24 (10024): 15–24.
- Taniguchi, M., H. Dulai, K.M. Burnett, I.R. Santos, R. Sugimoto, T. Stieglitz, G. Kim, N. Moosdorf, and W. Burnett. 2019. Submarine groundwater discharge: Updates on its measurement techniques, geophysical drivers, magnitudes, and effects. *Frontiers in Environmental Science* 7: 141.
- Virtasalo, J.J., J.F. Schröder, S. Luoma, J. Majaniemi, J. Mursu, and J. Scholten. 2019. Submarine groundwater discharge site in the First Salpausselkä ice-marginal formation, south Finland. *Solid Earth* 10 (2): 405–423.
- Wang, X., H. Li, J.J. Jiao, D.A. Barry, L. Li, X. Luo, C. Wang, L. Wan, X. Wang, X. Jiang, Q. Ma, and W. Qu. 2015. Submarine fresh groundwater discharge into Laizhou Bay comparable to the Yellow River flux. *Scientific Reports* 5 (1): 1–7.
- Wu, Z., H. Zhou, S. Zhang, and Y. Liu. 2013. Using ^{222}Rn to estimate submarine groundwater discharge (SGD) and the associated nutrient fluxes into Xiangshan Bay. *East China Sea. Marine Pollution Bulletin* 73 (1): 183–191.
- Zhang, Y., I.R. Santos, H. Li, Q. Wang, K. Xiao, H. Guo, and X. Wang. 2020. Submarine groundwater discharge drives coastal water quality and nutrient budgets at small and large scales. *Geochimica Et Cosmochimica Acta* 290: 201–215.